HHS Public Access

Author manuscript

Biomaterials. Author manuscript; available in PMC 2017 August 01.

Published in final edited form as:

Biomaterials. 2016 August ; 98: 53–63. doi:10.1016/j.biomaterials.2016.04.040.

In vivo fate tracking of degradable nanoparticles for lung gene transfer using PET and Ĉerenkov imaging

Kvar C.L. Black[1,‡], **Aida Ibricevic**[2,‡], **Sean P. Gunsten**[2], **Jeniree A. Flores**[4,5], **Tiffany P. Gustafson**[4,5], **Jeffery E. Raymond**[4,5,6], **Sandani Samarajeewa**[4], **Ritu Shrestha**[4], **Simcha E. Felder**[4], **Tianyi Cai**[2], **Yuefei Shen**[3], **Ann-Kathrin Löbs**[2], **Natalia Zhegalova**[1], **Deborah H. Sultan**[1], **Mikhail Berezin**[1], **Karen L. Wooley**[4,5,6], **Yongjian Liu**[1], and **Steven L. Brody**[1,2,*]

[1]Department of Radiology, Washington University, St. Louis, MO, 63110, USA

[2]Department of Internal Medicine, Washington University, St. Louis, MO, 63110, USA

[3]Department of Chemistry, Washington University, St. Louis, MO, 63110, USA

[4]Department of Chemistry, Texas A&M University, College Station, TX, 77843, USA

[5]Department of Chemical Engineering, Texas A&M University, College Station, TX, 77843, USA

[6]Laboratory for Synthetic-Biologic Interactions, Texas A&M University, College Station, TX, 77843, USA

Abstract

Nanoparticles (NPs) play expanding roles in biomedical applications including imaging and therapy, however, their long-term fate and clearance profiles have yet to be fully characterized *in vivo*. NP delivery *via* the airway is particularly challenging, as the clearance may be inefficient and lung immune responses complex. Thus, specific material design is required for cargo delivery and quantitative, noninvasive methods are needed to characterize NP pharmacokinetics. Here, biocompatible poly(acrylamidoethylamine)-*b*-poly(DL-lactide) block copolymer-based degradable, cationic, shell-cross-linked knedel-like NPs (Dg-cSCKs) were employed to transfect plasmid DNA. Radioactive and optical beacons were attached to monitor biodistribution and imaging. The preferential release of cargo in acidic conditions provided enhanced transfection efficiency compared to non-degradable counterparts. *In vivo* gene transfer to the lung was correlated with NP pharmacokinetics by radiolabeling Dg-cSCKs and performing quantitative biodistribution with parallel positron emission tomography and Čerenkov imaging. Quantitation of imaging over 14 days corresponded with the pharmacokinetics of NP movement from the lung to gastrointestinal and renal routes, consistent with predicted degradation and excretion. This ability to noninvasively and accurately track NP fate highlights the advantage of incorporating multifunctionality into particle design.

*Corresponding author: Fax 314-362-8987; brodys@wustl.edu.
‡These authors contributed equally

Keywords

degradable nanoparticle; biodistribution; cytotoxicity; lung; gene expression; Čerenkov luminescence imaging

INTRODUCTION

Multifunctional nanoparticles (NPs) offer a versatile platform to incorporate biologically-active and contrast-enhancing elements to create diagnostic, therapeutic, or theranostic agents[1–6]. NP-mediated nucleic acid delivery is one of the advancing applications for treatment of cancer[7–9] and non-malignant genetic diseases[10, 11]. The incorporation of cationic polymers into gene carriers has been particularly favorable due to their ability to efficiently complex anionic DNA by electrostatic interactions. Cationic polymers[12] such as poly(L-lysine)[13, 14], polyethylenimine (PEI)[15–18], dextran[19], and polyamidoamine (PAMAM) dendrimers[20, 21] have been used for nucleic acid delivery *in vivo*, however, clinical use has been limited by their toxicity[22]. Degradable nanomaterials may reduce toxicity and allow excretion of the degradation products after delivery of their payloads. NPs composed of poly(DL-lactide)[23, 24], poly(lactide-*co*-glycolide) (PLGA)[25, 26], and chitosan[27] have been widely used because of their enhanced biocompatibility and low toxicity, but tracking of their long term pharmacokinetic fate has not yet been fully explored. Hence, design and development of a NP system that allows multifunctionality such as binding to nucleic acid, imparting minimal toxicity, and providing the ability to track them is an important advance. Moreover, real-time monitoring of NP performance by *in vivo* imaging techniques could answer important questions regarding the delivery of therapeutic agents and subsequent NP fate.

The lung is an attractive but challenging organ for delivery of NPs. Anatomic advantages include ease of access *via* the airway and a large surface area for delivery and absorption. When properly functionalized, airway delivery of NPs may be used for treatment of lung diseases such as cystic fibrosis, cancer, and acute lung injury[28–31]. Gene delivery in the lung by NPs composed of PEI and tetrafunctional block copolymers[15–17, 32] has been achieved, and highly compact DNA NPs are able to pass the mucus barrier[33]. Beyond payload delivery, the fate and pharmacokinetics of the NP vehicles has not been evaluated, in part due to design limitations such as a lack of sensitive detection. Compared to systemic delivery by an intravenous route, tracking organ-specific delivery of NP vehicles is demanding, as an additional compartment must be included in any pharmacokinetic analysis. We and others have shown that NPs accumulate within the airways and alveolar air sacs, providing a potential depot effect for cargo release, and also impeding clearance or degradation that relies on extra-pulmonary metabolism or excretion[34, 35].

While long term tracking studies of NPs have been performed in tumor models[36–39] and after systemic injection of stem cells[40–42] labeled either with organic nanodots for optical imaging, or iron oxide-based NPs for magnetic resonance imaging (MRI), lung delivery remains less explored. The distribution of NPs delivered to the lung has been imaged by the co-administration of the conventional nuclear imaging agent ^{99m}Tc in combination with a

therapeutic nanoparticle for gene delivery[43]. However, there has been little investigation into the fate of degradable NPs after gene delivery to the lung using direct labeling of the NP and quantitative *in vivo* imaging over time to demonstrate organ distribution and clearance. Thus, our goal is the development of improved platforms and approaches to track the fate of NPs delivered to the lung.

To this end, multifunctional core-shell NPs capable of delivering therapeutic genetic materials to the airway have been explored. These NPs are composed of cationic block copolymers that self-assemble into core-shell micelles that can be covalently cross-linked into shell-cross-linked knedel-like NPs (cSCKs)[44, 45]. Designed to mimic natural DNA-binding histone proteins, these NPs have been used to deliver nucleic acids *in vitro*[46]. More recently, partially degradable cSCKs (Dg-cSCKs) with hydrolyzable poly(DL-lactide) in the core domain, a cleavable ester-based cross-linker throughout the shell region, and fluorescent tags for optical tracking were prepared and tested for delivery of siRNA *in vitro* in preliminary studies[47]. More important is their *in vivo* transfection performance with plasmid DNA (pDNA) and pharmacokinetic profiles, which have not been investigated. In this study, Dg-cSCKs were explored as a multifunctional NP platform to deliver pDNA, degrade, and be quantitatively tracked both *in vitro* and *in vivo* in mice. Given the specific features of NP degradation, we also focused on characterizing the *in vivo* pharmacokinetics and fate of the NP by radiolabeling Dg-cSCKs using a multimodal, noninvasive imaging approach that incorporated positron emission tomography (PET) and Čerenkov luminescence imaging.

MATERIALS AND METHODS

Detailed methods are included in the Supporting Information (SI).

Synthesis of degradable cSCKs

The synthesis of non-degradable cSCKs (NonDg-cSCKs) and labeling with Alexa Fluor 647 is previously described[44, 45]. Synthesis of degradable cSCKs (Dg-cSCKs) and production of cSCK labeled with Alexa Fluor succinimidyl ester (Life Technologies, Grand Island, NY) were recently reported[47]. Physical characterization of cSCKs, including hydrodynamic diameter (D_h), size distributions of cSCK and zeta potential measurements were determined as described[48] and as detailed in the SI.

Plasmid DNA preparation

Plasmids pEGFP-N1 (Clontech Laboratories, Mountain View, CA, referred to as pGFP) and pGL4.51 (Promega, Madison, WI, referred to as pLuc), were used to express enhanced green fluorescent protein (eGFP) and firefly (Photinus pyralis) luciferase, respectively, each under control of a cytomegalovirus gene (CMV) promoter. Plasmid DNA was isolated and purified using the Qiagen EndoFree Plasmid kit (Qiagen, Valencia, CA).

cSCK binding to plasmid DNA

pGFP was diluted to 0.2 μg/10 μL and mixed with cSCK at different ratios of NP amine (N) to plasmid DNA phosphate (P) (N/P). cSCK:pGFP complexes were incubated in PBS buffer

for 30 minute and resolved by electrophoresis on a 1 percent agarose gel where DNA was visualized by ethidium bromide staining[44].

Halogen radiolabeling Dg-cSCKs

^{123}I, ^{124}I, ^{131}I, and ^{76}Br radiolabeling of Dg-cSCK are described in the SI. Radiochemical purity was determined by radio-thin layer chromatography. The radioiodination of the Dg-cSCKs was optimized using ^{123}I. The biodistribution, PET and Čerenkov imaging were performed with ^{124}I radiolabeling, which was further confirmed by ^{131}I labeling (Table 1).

NP degradation assay

PBS (250 μL, pH 7.4) was added to a lyophilized vial of Dg-cSCK for a final concentration of 2 mg/mL. The solution was sonicated for 5 minutes, and 50 μL was added to an iodination tube containing 18.0 MBq of ^{124}I (3D Imaging, Maumelle, AR) in 100 μL of PBS. Following incubation at room temperature for 20 minutes, the labeling efficiency was determined by radio-TLC and confirmed to be > 95 percent. The sample was analyzed 1 hour and 7 days after dissolution on a GE ÄKTA fast protein liquid chromatography (FPLC) system using a Tosoh TSK gel PW XL-CP cationic exchange column equipped with a FW XL-CP guard column. Samples were run at 0.8 mL/min in SEC buffer with individual 0.8 mL fractions collected. These fractions were then analyzed on a gamma counter (Perkin Elmer, Waltham, MA). The CPM were plotted to generate the elution profile of the ^{124}I-labeled Dg-cSCK.

Characterization of cSCK:pDNA nanocomplexes

Nanocomplexes were characterized using dynamic light scattering (DLS), transmission electron microscopy (TEM), and atomic force microscopy (AFM) as described in the SI.

NP cytotoxicity

HEK293T cells were cultured using standard methods. cSCKs over a range of concentrations were incubated with cells for 24 h. Cell ATP activity was measured as a marker of cell viability using the Cell-Titer-Glo Reagent (Promega, Madison, WI).

In vitro transfection assay

HEK293T cells were cultured in 96-well plates for 18 hours before transfection. Transfectant solutions were sonicated then added to opti-MEM media, mixed, and incubated for 5 minutes. pGFP or pLuc was added to achieve specific N/P ratios and incubated for 30 minutes at room temperature ([DNA] = 2 μg/mL; [NonDg-cSCK] = 4.32 to 17.28 μg/mL; [Dg-cSCK] = 12 to 36 μg/mL). For GFP expression, HEK293T cells were analyzed by flow cytometry. Luciferase activity was measured by the Luciferase Assay system using the manufacturer's protocol (Promega). The measure of luciferase activity relative to ATP cytotoxicity was determined as a measure of the utility of the NP as a transfectant.

Flow cytometry

HEK293T cell entry of cSCKs labeled with Alexa Fluor 647 was quantified by flow cytometry using a FACSCalibur flow cytometer (BD Biosciences, San Jose, CA). The

percent cells expressing Alexa Fluor 647 and median fluorescent intensity (MFI) were determined using CELLquest software (BD Biosciences, San Diego, CA).

In vitro imaging of pDNA and cSCKs

pDNA was labeled with FITC using the Label IT Tracker Kit (Mirus Bio, Madison, WI). To confirm colocalization of cSCKs with endosomes, HEK293T cells were labeled with early endosome marker Rab5a (Cell Light Early Endosomes-RFP BacMam 2.0, Life Technologies, Grand Island, NY).

DNA release assay

GelRed dye (Biotium, Hayward, CA) was used to report free DNA released from NP:pDNA complexes. GelRed was diluted in PBS to make a stock solution of 0.25 mg/mL. Solutions of NP with and without pDNA were incubated at 37 °C for either 4 or 24 h (at either pH 5 or 7) prior to addition of GelRed dye solution. Fluorescence spectra were recorded on a Nanolog VIS-NIR spectrofluorometer (Horiba, Kyoto, Japan) equipped with a double grating monochromator iHR320 imaging spectrograph, and a thermoelectrically cooled (−25 °C) R928P photomultiplier tube as a detector. GelRed dye (20 μL) was added to each cuvette containing 1 mL of cSCK or cSCK:pDNA complexes and fluorescence intensity was measured at 430 nm excitation and 510–700 nm emission, with both slits at 5 nm, and integration time 0.2 sec. FluorEssence (Horiba, Kyoto, Japan) software was used to operate the fluorimeter and process the data.

In vivo NP:pDNA nanocomplex delivery and transfection assay

The Animal Studies Committee of the Washington University approved all animal studies reported. Mice were administered NP:pDNA nanocomplexes by way of a percutaneous catheter inserted into the trachea of sedated animals[34]. Dg-cSCK:pLuc nanocomplexes were freshly prepared, using an N/P ratio of 8:1 and administered intratracheally as a single 50 μL volume ([DNA] = 15 to 35 μg; [Dg-cSCK] = 72 to 168 μg). Control mice were treated with water, pLuc only (25 μg), or with a complex of pLuc (25 μg) and 2 μL stock polyethylenimine solution **(**PEI, Polyplus, Illkirch, FR**)**. Lungs were homogenized and assayed for DNA transfection efficiency by measuring luciferase activity as *in vitro*. Luciferase activity was normalized to the protein content (RLU/mg protein).

Bronchoalveolar lavage (BAL) and lung tissue histology

To obtain BAL fluid cells to characterize inflammatory response, mice were euthanized, and lung lavage was performed as previously described[34]. Total cells recovered by BAL were quantified and cell differential determined using standard light microscopy criteria. Following BAL, lungs were inflation fixed, embedded in paraffin and tissue sections obtained for hematoxylin and eosin staining.

Biodistribution and excretion

Dg-cSCKs radiolabeled with ^{76}Br, ^{124}I, or ^{131}I and complexed with pDNA were administered intratracheally (0.19 to 0.37 MBq per mouse). Organs were weighed and analyzed by gamma counter (Model 8000, Beckman, Brea, CA) as described[34, 49].

Standards were measured in parallel to calculate the percentage injected dose per gram of tissue (percent ID/g) or per organ of tissue (percent ID/organ)[34, 49–51]. Urine and feces were collected every 2 days and assayed by gamma counter to determine excretion.

PET imaging

A suspension of ^{76}Br-labeled Dg-cSCKs or ^{124}I-labeled Dg-cSCK:pLuc nanocomplex was administered to lungs intratracheally (1.85 MBq/mouse). PET and corresponding x-ray computed tomography (CT) images were acquired using cross-calibrated Inveon microPET/CT (Siemens, Munich, Germany) or Focus 220 PET (Concorde Microsystems, Knoxville, TN) scanners. Acquisition times ranged from 15 to 60 minutes. Standardized uptake values (SUVs) from the lungs were quantified by image analysis with Inveon software (Siemens).

Čerenkov luminescent imaging

Mice used for biodistribution or PET imaging were also imaged by detection of Čerenkov radiation from either ^{124}I- or ^{131}I-labeled cSCK:pDNA complexes. After intratracheal injection, mice were imaged with an optical IVIS 100 Spectrum system (Perkin Elmer, Waltham, MA) for 10 minutes. Radiances (p/s/cm^2/sr) from lung regions of interest were quantified with Living Image 3.0 software (Caliper Life Sciences, Hopkinton, MA). To normalize radiant intensities, background luminescent signal was subtracted and signals were corrected for ^{124}I or ^{131}I radioactive decay.

Statistical analysis

Unpaired samples were compared using the 2-tailed Student's *t*-test. The level of significance was set at $p < 0.05$.

RESULTS AND DISCUSSION

Dg-cSCK synthesis and halogen radiolabeling

The SCKs composed of block co-polymers have been created as an adaptable class of vehicles for *in vitro* and *in vivo* delivery of theranostic agents[44, 45]. For these studies, as an alternative to previous nondegradable cSCKs (NonDg-cSCK)[46], the block co-polymers were altered to incorporate degradable ester bonds in the hydrophobic component while keeping the positively-charged outer shell for nucleic acid carriage and intracellular uptake[47]. To track the NPs, fluorescent markers and hydroxyphenyl rings for halogen radiolabeling were added. Dg-cSCKs (Figure 1A) were synthesized as previously described[47] to generate NPs with a hydrodynamic diameter ($D_{h(number)}$) of 135 ± 40 nm as measured by DLS. The shell of these cSCKs possessed the positive charge necessary for DNA complexation, as indicated by a zeta potential surface charge of *ca.* + 40 mV.

To impart multifunctional imaging properties to the Dg-cSCK for *in vitro* and *in vivo* tracking studies and pharmacokinetic characterization, the NPs were labeled either with Alexa Fluor 647[44, 45] or radiohalogens. Radiolabeling with each radionuclide (^{123}I, ^{124}I, ^{131}I, and ^{76}Br) was achieved by means of a hydroxyphenyl ring introduced within the shell of the cSCK. Radiolabeling with ^{76}Br was used for an initial assessment of

biodistribution and PET imaging of NP alone. We chose Br is it is easily available at our institution, and offers the ability to rapidly perform both biodistribution and high resolution PET imaging[34]. ^{123}I was employed to optimize radiochemistry since it was the most economical nuclide, ^{124}I was used to provide multimodal imaging and biodistribution functionality, and ^{131}I was used to confirm the results by mitigating potential for radiolysis from ^{124}I high-energy radiation (Table 1). The ^{123}I-tagged Dg-cSCK demonstrated high labeling efficiency and radiochemical purity that were ratio dependent (Figure 1B) wherein higher Dg-cSCK:^{123}I ratios provided greater radiochemical purity, but lower specific activity. The specific activities were consistent with prior NP radiolabeling studies for tumor imaging[52]. The inclusion of the radionuclides provided the ability to radiolabel Dg-cSCKs for quantitative biodistribution and excretion studies *in vivo*, which are necessary to understand the biologic function of this particular nanomaterial in whole animal models.

Dg-cSCKs degradation in aqueous solutions

We hypothesized that cSCKs with degradable ester bond crosslinkers (Dg-cSCKs) would enhance clearance and decrease toxicity. Balancing the rate of degradation with toxicity was of interest, since immediate degradation may prevent payload delivery while a prolonged dissolution could increase inflammation. Dg-cSCK degradation in aqueous conditions was characterized using ^{124}I-labeled NP suspensions injected into a highly sensitive radioactive size exclusion column at early and late time points (Figure 1C). Only one peak was present one hour after dissolution (8 mL elution volume), representative of a single cSCK species. In contrast, 7 days after dissolution, the peak at 8 mL was significantly diminished, indicating some remaining intact Dg-cSCK. However, multiple new, prominent peaks were observed between 10 and 20 mL, which is consistent with the observation lactic acid and different sized oligo(lactic acid) were released from the original Dg-cSCK as a result of ester bond degradation[47, 53]. Importantly, these degradative products could be detected with greater sensitivity than in previous studies of degradation performed on these Dg-cSCKs.

Degradable cSCKs bind DNA and form nanocomplexes

Effective NP-mediated gene transfer requires high pDNA binding and efficient intracellular delivery. We have previously demonstrated that the NonDg-cSCKs efficiently transfect siRNA[54] and peptide nucleic acid (PNA)[45] *in vitro* by means of the cationic shell, however pDNA transfection was never evaluated. The poly(acrylamidoethylamine)-based cationic shell of the Dg-cSCKs was designed to bind pDNA through electrostatic interaction with amines (Figure 1A). The DNA binding of the non-degradable and Dg-cSCK were compared over a range of molar cSCK amine to pDNA phosphate (N/P) ratios (1:1 to 16:1). Both types of NP complexed with pDNA (pGFP) at N/P ratios of 2:1 and above (Figure 1D). Non-complexed Dg-cSCKs ranged in size from 25–50 nm by TEM (Figure 1E), and aggregation was observed that led to particle sizes ~ 100 nm (Figure 1E inset), consistent with the sizes detected by DLS. Dg-cSCK:pGFP nanocomplexes at the N/P ratio of 8:1 were characterized by TEM and DLS. TEM revealed a wide variation in nanocomplex size and shape (Figure 1F), and DLS displayed a doubling of size and polydispersity compared to the cSCKs alone ($D_{h(number)}$ = 240 ± 60 nm; Figure S1A), which was confirmed with atomic force microscopy (AFM; Figure S1B). Using AFM under wet conditions *in situ*, particle diameter increased by 20 percent between minute 5 and 10, while the surface roughness

decreased by 10 percent, which we propose is due to dynamic reorganization events of the nanocomplexes formed between Dg-cSCKs and pDNA and the presence of non-crosslinked transient polymer. This NP:pDNA complex is consistent with the dynamic physicochemical interactions of nucleic acids with other NPs and lipid moieties used for efficient gene delivery[55, 56].

In vitro transfection efficiency of Dg-cSCK

In addition to binding DNA, the cationic shell of the cSCK may also provide the capacity for cell uptake, potentially through electrostatic interaction with negatively-charged cell membranes, another required step for successful gene delivery. First, *in vitro* transfer of the previously efficacious NonDg-cSCK[46] was compared with the Dg-cSCK using gene expression reporter plasmids for eGFP and luciferase expression (Figures 2A, 2B, and S2A) in the mammalian epithelial cell line, HEK293T. Transfection of pGFP and pLuc with Dg-cSCK complexes provided 200 and 300 percent greater transfection efficiency, respectively, when compared to NonDg-cSCKs, and Dg-cSCKs provided 30 percent greater efficiency than commercial transfectant Lipofectamine2000. The peak activities were at N/P ratios of 20:1 for NonDg-cSCKs and 30:1 for Dg-cSCKs. A significant decrease in cell viability was seen above these high ratios (Figures 2A and S2B). Therefore, nontoxic N/P ratios of 15:1 for NonDg-cSCK and 20:1 for Dg-cSCK were chosen for further study *in vitro*.

pH-dependent pDNA release from cSCK:pDNA nanocomplexes

Next, the mechanisms accounting for the enhanced Dg-cSCK-mediated gene transfer compared to NonDg-cSCKs were explored. To monitor each component of the NP complex independently during cell uptake, the polymer strands of the cSCKs were tagged with Alexa Fluor 647 while pDNA was labeled with FITC. The cell uptake of NonDg-cSCKs and Dg-cSCKs were similar either alone or in complex with DNA, both occurring within 90 minutes (Figure S3A). Also, characterization of intracellular trafficking of labeled cSCK and pDNA by confocal microscopy showed that complexes of each NP type were similarly localized in endosomes 4 hours after initial incubation (Figure S3B), suggesting that improved intracellular trafficking was also not the cause of the difference in transfection efficiency. However, there was significantly higher luciferase activity in cells transfected with similar amounts of pLuc carried by Dg-cSCK compared to NonDg-cSCK at 40 hours post-incubation and later (Figure 2B). These findings suggested that the difference in gene delivery efficiency occurs after the nanocomplexes have reached the endosomes.

Thus, it was hypothesized that differences in intracellular release of pDNA from the cSCK was the cause of the enhanced gene expression observed with the degradable nanocarrier. Therefore, cSCK:pDNA complexes were incubated with GelRed, a dye that changed emission spectrum after binding free DNA. At 24 hours after nanocomplex incubation at pH 7.0, pDNA complexed with Dg-cSCK demonstrated significantly higher amounts of free DNA compared to NonDg-cSCK:pDNA complexes (Figure 2C). Moreover, this difference was substantially greater at pH 5.0 (Figure 2D). These observations supported the proposition that Dg-cSCKs degrade, releasing lactic acid byproducts and altering the integrity of the cationic shell, leading to the release of pDNA cargo more efficiently in acidic endosomes compared to their NonDg-cSCK counterparts. It is also possible that after

cellular uptake, the lactic acid release may also lower the intracellular pH of cells, further enhancing the pH-dependent pDNA release.

In vivo gene transfection

This was the first study to evaluate the *in vivo* transfection performance of Dg-cSCKs; specifically, Dg-cSCK:pLuc nanocomplexes were assessed after delivery to the airway in mice. Nanocomplexes with a range of N/P ratios (1:1, 3:1, 6:1 and 8:1) were administered intratracheally and luciferase expression was quantified in whole lung homogenates. The ratio of Dg-cSCK to pLuc resulting in the highest level of gene expression (8:1 ratio) was used in combination with 25 μg of pDNA for subsequent experiments (Figure 3A). As expected, using a conventional pDNA vector, the luciferase activity was transient, with the highest expression observed at day 2 (the earliest time point examined), then declined by days 7 and 14 (Figure S4). The peak luciferase expression of the lungs treated with Dg-cSCK:pLuc nanocomplexes was 8-fold higher than the effect of naked pDNA. The levels of Dg-cSCK-mediated pDNA luciferase activity was similar to some reports of NP-mediated transfection in the lung, while lower than others[11, 14]. Lungs treated with Dg-cSCK:pLuc nanocomplexes had 10-fold lower luciferase activity than lungs from animals treated with the commercial *in vivo* transfectant PEI in complex with pLuc, though the PEI reagent induced epithelial necrosis, peribronchial and alveolar inflammation as reported[57, 58]. Dg-cSCK:pDNA resulted in a mild inflammatory response compared to PEI alternatives, as determined by bronchoalveolar lavage (BAL) inflammatory cells (Figure 3B). Alveolar infiltrates were not observed in the lungs of mice treated with Dg-cSCK:pDNA nanocomplexes. While Dg-cSCK has the capacity for successful *in vivo* gene delivery, it is also possible that Dg-cSCK carriage of new generation minicircle DNA plasmids lacking prokaryotic sequences or plasmids with eukaryotic promoters would enhance both levels and maintenance of gene expression[59, 60]. Due to its relative biocompatibility, gene transfer potential, and degradability, therapeutic plasmids such as those for modulating infection, inflammation or fibrosis could be delivered in an identical manner as pLuc in this study to provide therapy for acute (e.g., respiratory virus infection) and chronic (e.g., pulmonary fibrosis) lung diseases with minimal adverse effects from the nanocarrier[10, 11].

Biodistribution of Dg-cSCK:pDNA complex clearance *in vivo*

We next sought to characterize NP-nucleic acid conjugate pharmacokinetics, as would be required for future translation. Short term gene delivery to the lung with nanocarriers has been characterized with nuclear and optical imaging[43], and nanoprobes have been used in a variety of modalities for long term stem cell and tumor tracking[36–40]. However, these studies are often hampered by low sensitivity or limited by tissue attenuation that make multi-organ quantitative biodistribution studies difficult, and the long term *in vivo* fate of gene-delivering nanocarriers indefinite. In our study using the radiolabeling functionality of the Dg-cSCKs, NPs labeled with different radioisotopes were evaluated in biodistribution studies and whole animal imaging.

We initially assessed the biodistribution using a short-lived ^{76}Br-labelled Dg-cSCKs (Figure S5) that also enabled simultaneous PET. Biodistribution and imaging provided evidence of lung clearance over 48 hours ($p < 0.05$), accompanied by clearance through the

gastrointestinal tract, though the short half-life did not allow us to track subsequent clearance. Therefore, to facilitate both long term quantitative biodistribution and noninvasive PET imaging, and characterize the pharmacokinetics of the Dg-cSCKs:pDNA complexes, NPs were radiolabeled with the β^+ emitting PET isotope ^{124}I and tracked for 14 days (Figure 4). Initially, Dg-cSCKs were highly retained in the lung, with 40.0 percent ID/organ present 1 hour after intratracheal delivery, and then significantly decreased over time (Figure 4A). Within the lung, there was evidence that a portion of the uptake was in lung immune cells as indicated by activity in cells recovered by BAL (Figure 4B). This was observed at 1 hour (6.0 percent ID/organ), 1 day (9.8 percent ID/organ) and up to 7 days post-delivery, diminishing as the complexes, and possibly the cells were cleared from the lung.

Both renal and gastrointestinal clearance of Dg-cSCKs:pDNA complexes were observed (Figure 4A). Blood pool and renal clearance was highest within an hour after delivery (6.6 %ID/organ total), then decreased significantly at later times, representing rapid clearance of portions of the cSCK:pDNA nanocomplexes through the kidney and bladder or the deiodination of the ^{124}I radiolabel indicated by the thyroid accumulation (Table S1). Significant activity was observed in the gastrointestinal tract at both 1 hour (17.3 %ID/organ) and 1 day (11.7 %ID/organ). The degree of initial activity significantly dropped 72 hours after injection (1.9 %ID/organ) and continued at low levels throughout the study. Similar trends were observed when the data were represented as percent ID/g of tissue (Table S1).

Complementary activity was detected in excreted urine and feces (Figure 4C and S6). A significant amount of the total radioactive signal excreted in the urine occurred within 48 hours (25.8 percent ID), further increasing to a total of 52.9 percent ID over 4 days, then dropping off significantly at later time points. Renal clearance may represent rapid and sustained breakdown of particles that reach systemic circulation through alveolar-capillary transit since there was low deiodination as indicated by minimal thyroid accumulation[61]. Excretion through the GI system was comparatively less but also cleared mainly in the first 4 days post-delivery. Within 2 days, 4.8 percent ID was excreted, reaching a total of 10.4 percent ID after 4 days, suggesting continued mucociliary clearance or hepatobiliary clearance with secretion into the intestine. Mucociliary clearance of particles over 100 nm is well known and movement of NPs from the airway into the posterior pharynx and the gastrointestinal tract was previously reported[34, 62]. A total of 65.8 percent ID was excreted through both urine and feces in 7 days. The clearance kinetics observed were significantly slower from the lung compared to a recent study that used either NPs of 34 nm or less than 5 nm, which may be attributed to the significantly larger sizes, charge, or composition of the cSCK:pDNA nanocomplexes[61].

To confirm the ^{124}I studies, ^{131}I with low decay energy to mitigate radiolysis of the NP by ^{124}I radiation was used. Accordingly, Dg-cSCKs were labeled with ^{131}I, complexed with pDNA, and tracked for 14 days after intratracheal injection (Figure S7). Like the ^{124}I studies, ^{131}I-labeled Dg-cSCK:pDNA complexes significantly cleared from the lung. By day 14, 8-fold less radioactivity was present in the lung compared to 1 hour after injection, and evidence of both renal and hepatobiliary clearance was observed.

Multimodal imaging of Dg-cSCK fate

The ability to noninvasively track NP pharmacokinetics is another goal for assessing the utility of clinical nanomaterial-based therapeutics. Therefore, the value of noninvasive PET and *in vivo* optical imaging to characterize the clearance and excretion of the Dg-cSCK:pDNA complexes was investigated.

To correlate noninvasive PET with biodistribution, PET/CT was performed after intratracheal injection of the ^{124}I-labeled Dg-cSCK:pDNA nanocomplexes (Figure 5A–C). Substantial activity was observed in the lung and tracheal injection site 1 hour post-delivery. In PET images, SUVs from whole lungs decreased from 5.4 ± 1.0 to 3.8 ± 0.9 between 1 hour and 1 day after administration ($p = 0.029$; $n = 8$), then decreased to 30 percent of its original value at 14 days (Figure 5E; $n = 8$, $p < 0.00001$), mirroring the biodistribution pharmacokinetics. Lung clearance profiles measured by changes in biodistribution percent ID/organ values were highly correlated with the decrease in PET signal SUV ($r^2 = 0.99$). Although difficult to quantify within the abdomen, like the biodistribution data, PET signal was evident in the gastrointestinal tract 1 hour and 1 day after injection, and decreased over time. These findings suggest that imaging could be used to track the biodistribution of these NPs.

Čerenkov luminescent imaging is an emerging modality used with NP imaging as an alternative to nuclear imaging[63–65]. Čerenkov images can be acquired using standard IVIS optical imaging hardware rather than PET/CT systems, expanding accessibility and the possibilities for high throughput screening. This modality was explored to noninvasively image NP clearance from the lung using both PET and non-PET radionuclides as Čerenkov radiation from either of these isotopes can be imaged. Čerenkov images of mice receiving intratracheal ^{124}I- or ^{131}I-labeled Dg-cSCK:pDNA complexes were generally similar to PET active isotopes (Figures 5D and 6). Both PET and Čerenkov imaging modalities provided similar clearance profiles of the ^{124}I-labeled cSCK:pDNA complexes from the lung over time (Figures 5E and F). When imaging the ventral surface of mice, Ĉerenkov imaging provided confirmation of mucociliary clearance and subsequent gastrointestinal clearance, with radiance transferring from the lung to the gastrointestinal tract between the time of initial administration and 3 days later (Figure 6). Radiance values from lung regions of interest in Čerenkov images correlated closely with lung PET SUV values. After subtracting background signal and normalizing to ^{124}I decay, lung radiance values decreased from 5.4 to 2.4×10^5 p/s/cm^2/sr throughout the 14 days (r^2=0.99, SUV *vs.* normalized radiance).

Our findings imply that both optical Čerenkov luminescence and PET imaging can be used to characterize delivery and clearance of NPs into and from the lungs of small animals. While Čerenkov radiation is limited by common optical challenges such as poor tissue penetration, these data imply that it can be used to characterize the delivery and clearance of radiolabeled NPs from the lung and potentially other organs in mouse models, and for selective applications in larger animals. Due to its ability to bridge nuclear imaging modalities such as PET and single-photon emission computed tomography (SPECT) with optical imaging counterparts, Čerenkov radiation has the potential to play an active role in aiding the translation of pre-clinical small animal studies to clinically relevant human trials without a change in particle composition.

CONCLUSIONS

In this study, degradable positively-charged polymer NPs were designed with the capacity for multifunctionality including gene delivery, degradability, and both radionuclide and optical imaging to determine the noninvasive long-term performance and pharmacokinetics following airway delivery to the lung. Degradable cSCKs provided enhanced gene transfer compared to non-degradable alternatives through enhanced pDNA release in acidic pH conditions found in intracellular compartments, and caused less toxicity compared to more common carriers like PEI, making them a promising platform to deliver genetic materials. An *in vivo* pharmacokinetic profile was determined by tracking radiolabeled Dg-cSCK:pDNA complexes using biodistribution studies and noninvasive imaging. The findings were compatible with the degradation of the NP observed *in vitro*, suggesting that chemical design and characterization assays were valid predictors of performance. As predicted, the unique anatomic and physiologic features of the airway and alveolar airspaces resulted in a prolonged decline in lung residence; quantitative biodistribution studies precisely identified resultant NP pharmacokinetics of both blood and intestinal clearance, which may be unique to airway-delivered NPs. More importantly, both preclinical PET and Čerenkov imaging correlated strongly with the biodistribution results, indicating that noninvasive methods can be used to image organs of distribution to track the real-time clearance of nanocomplexes in a semi-quantitative fashion. In future studies, tracking biologically active payloads could be additionally correlated to the NP pharmacokinetics. Overall, the multimodal Dg-cSCK NP allowed manipulation of core building blocks to customize cargo delivery while simultaneously allowing the addition of multiple types of beacons for noninvasive *in vivo* tracking. These NPs are promising candidates for clinical translation, and our strategy to study long-term fate of the particles is adaptable for other materials delivered *in vivo*.

Supplementary Material

Refer to Web version on PubMed Central for supplementary material.

Acknowledgments

This work was supported by the National Heart, Lung, and Blood Institute Program in Excellence in Nanotechnology (NHLBI PEN; HHSN268201000046C); the Welch Foundation through the W. T. Doherty-Welch Chair in Chemistry to KLW (grant number A-0001) and the Barnes-Jewish Hospital Research Foundation through the Dorothy R. and Hubert C. Moog Chair in Pulmonary Medicine to SLB. We thank the Washington University Pre-Clinical Imaging Facility for assistance with the biodistribution, PET imaging, and excretion studies, the Washington University Center for Cellular Imaging for assistance with TEM, and the Microscopy Imaging Center at Texas A&M University.

References

1. Jokerst J, Lobovkina T, Zare R, Gambhir S. Nanoparticle PEGylation for imaging and therapy. Nanomedicine. 2011; 6:715–28. [PubMed: 21718180]
2. Guo Y, Aweda T, Black K, Liu Y. Chemistry and theranostic applications of radiolabeled nanoparticles for cardiovascular, oncological, and pulmonary research. Curr Top Med Chem. 2013; 13:470–8. [PubMed: 23432009]
3. Sanvicens N, Marco M. Multifunctional nanoparticles – properties and prospects for their use in human medicine. Trends in Biotechnology. 2008; 26:425–33. [PubMed: 18514941]

4. Cheng Z, Zaki A, Hui J, Muzykantov V, Tsourkas A. Multifunctional Nanoparticles: Cost Versus Benefit of Adding Targeting and Imaging Capabilities. Science. 2012; 903:903–10. [PubMed: 23161990]
5. Kim T, Lee S, Chen X. Nanotheranostics for personalized medicine. Expert Rev Mol Diagn. 2013; 13:257–69. [PubMed: 23570404]
6. Jia, F.; Liu, X.; Li, L.; Mallapragadaa, S.; Narasimhana, B.; Wang, Q. Multifunctional nanoparticles for targeted delivery of immune activating and cancer therapeutic agents. J Control Release. 2013. http://dx.doi.org/10.1016/j.jconrel.2013.10.012
7. Kenny G, Villegas-Llerena C, Tagalakis A, Campbell F, Welser K, Botta M, et al. Multifunctional receptor-targeted nanocomplexes for magnetic resonance imaging and transfection of tumours. Biomaterials. 2012; 33:7241–50. [PubMed: 22809644]
8. Iyer A, Duan Z, Amiji M. Nanodelivery systems for nucleic acid therapeutics in drug resistant tumors. Mol Pharm. 2014; 11:2511–26. [PubMed: 24661041]
9. Guerrero-Cázares H, Tzeng S, Young N, Abutaleb A, Quiñones-Hinojosa A, Green J. Biodegradable Polymeric Nanoparticles Show High Efficacy and Specificity at DNA Delivery to Human Glioblastoma in Vitro and in Vivo. ACS Nano. 2014; 8:5141–53. [PubMed: 24766032]
10. da Silva A, Martini S, Abreu S, Samary C, Diaz B, Fernezlian S, et al. DNA Nanoparticle-Mediated Thymulin Gene Therapy Prevents Airway Remodeling in Experimental Allergic Asthma. J Control Release. 2014; 180:125–33. [PubMed: 24556417]
11. Suk J, Kim A, Trehan K, Schneider C, Cebotaru L, Woodward O, et al. Lung Gene Therapy with Highly Compacted DNA Nanoparticles that Overcome the Mucus Barrier. J Control Release. 2014; 178:8–17. [PubMed: 24440664]
12. Pack D, Hoffman A, Pun S, Stayton P. Design and development of polymers for gene delivery. Nat Rev Drug Discov. 2005; 4:581–93. [PubMed: 16052241]
13. Ziady A, Gedeon C, Miller T, Quan W, Payne J, Hyatt S, et al. Transfection of airway epithelium by stable PEGylated poly-L-lysine DNA nanoparticles in vivo. Mol Ther. 2003; 8:936–47. [PubMed: 14664796]
14. Boylan N, Kim A, Suk J, Adstamongkonkul P, Simons B, Lai S, et al. Enhancement of airway gene transfer by DNA nanoparticles using a pH-responsive block copolymer of polythylene glycol ond poly-L-lysine. Biomaterials. 2012; 33:2361–71. [PubMed: 22182747]
15. Gautam A, Densmore C, Golunski E, Xu B, Waldrep J. Transgene Expression in Mouse Airway Epithelium by Aerosol Gene Therapy with PEI-DNA Complexes. Mol Ther. 2001; 3:551–6. [PubMed: 11319917]
16. Rudolph C, Ortiz A, Schillinger U, Jauernig J, Plank C, Rosenecker J. Methodological optimization of polythylenimine (PEI)-based gene delivery to the lungs of mice via aerosol application. J Gene Med. 2005; 7:59–66. [PubMed: 15538727]
17. Zamora-Avila D, Zapata-Benevides P, Franco-Molina M, Saavedra-Alonso S, Trejo-Avila L, Resenez-Perez D, et al. WT1 gene silencing by aerosol delivery of PEI-RNAi complexes inhibits B16-F10 lung metastases growth. Cancer Gene Therapy. 2009; 16:892–9. [PubMed: 19461674]
18. Kleemann E, Neu M, Jekel N, Fink L, Schmehl T, Gessler T, et al. Nano-carriers for DNA delivery to the lung based upon a TAT-derived peptide covalently coupled to PEG–PEI. J Control Release. 2005; 109:299–316. [PubMed: 16298009]
19. Abdullah S, Wendy-Yeo W, Hosseinkhani H, Hosseinkhani M, Masrawa E, Ramasamy R, et al. Gene Transfer into the Lung by Nanoparticle Dextran-Spermine/Plasmid DNA Complexes. Journal of Biomedicine and Biotechnology. 2010; 2010:1–10.
20. Navarro G, Maiwald G, Haase R, Rogach A, Wagner E, Ilarduya CTD, et al. Low generation PAMAM dendrimer and CpG free plasmids allow targeted and extended transgene expression in tumors after systemic delivery. J Control Release. 2010; 146:99–105. [PubMed: 20438778]
21. Arima H, Yamashita S, Mori Y, Hayashi Y, Motoyama K, Hattori K, et al. In Vitro and In Vivo gene delivery mediated by Lactosylated Dendrimer/α-Cyclodextrin Conjugates (G2) into Hepatocytes. J Control Release. 2010; 146:106–17. [PubMed: 20678990]
22. Li C, Liu H, Sun Y, Wang H, Guo F, Rao S, et al. PAMAM nanoparticles promote acute lung injury by inducing autophagic cell death through the Akt-TSC2-mTOR signaling pathway. J Mol Cell Biol. 2009; 1:37–45. [PubMed: 19516051]

23. Zhao Y, Fu J, Ng D, Wu C. Formation and Degradation of Poly(D,L-lactide) Nanoparticles and Their Potential Application as Controllable Releasing Devices. Macromol Biosci. 2004; 4:901–6. [PubMed: 15468299]
24. Ataman-Önal Y, Munier S, Ganée A, Terrat C, Durand P, Battail N, et al. Surfactant-free anionic PLA nanoparticles coated with HIV-1 p24 protein induced enhanced cellular and humoral immune responses in various animal models. J Control Release. 2006; 112:175–85. [PubMed: 16563545]
25. Kim J, Park J, Yang H, Woo D, Jeon S, Do H, et al. The use of biodegradable PLGA nanoparticles to mediate SOX9 gene delivery in human mesenchymal stem cells (hMSCs) and induce chondrogenesis. Biomaterials. 2011; 32:268–78. [PubMed: 20875683]
26. Vij N, Min T, Marasigan R, Belcher C, Mazur S, Ding H, et al. Development of PEGylated PLGA nanoparticle for controlled and sustained drug delivery in cystic fibrosis. J Nanobiotechnology. 2010; 8
27. Roy K, Mao H, Huang S, Leong K. Oral gene delivery with chitosan-DNA nanoparticles generates immunologic protection in a murine model of peanut allergy. Nat Med. 1999; 5:387–91. [PubMed: 10202926]
28. Sung J, Pulliam B, Edwards D. Nanoparticles for drug delivery to the lungs. Trends in Biotechnology. 2007; 25:563–70. [PubMed: 17997181]
29. Yang W, Peters J, W R III. Inhaled nanoparticles-A current review. Int J Pharm. 2008; 356:239–47. [PubMed: 18358652]
30. Mansour H, Rhee Y, Wu X. Nanomedicine in pulmonary delivery. Int J Nanomedicine. 2009; 4:299–319. [PubMed: 20054434]
31. Roy I, Vij N. Nano-delivery in Airway Diseases: Challenges and Therapeutic Applications. Nanomedicine. 2010; 6:237–44. [PubMed: 19616124]
32. Richard-Fiardo P, Hervouet C, Marsault R, Franken P, Cambien B, Guglielmi J, et al. Evaluation of tetrafunctional block copolymers as synthetic vectors for lung gene transfer. Biomaterials. 2015; 45:10–7. [PubMed: 25662490]
33. Mastorakos P, da Silva A, Chisholm J, Song E, Choi W, Boyle M, et al. Highly compacted biodegradable DNA nanoparticles capable of overcoming the mucus barrier for inhaled lung gene therapy. Proc Natl Acad Sci U S A. 2015; 112:8720–5. [PubMed: 26124127]
34. Liu Y, Ibricevic A, Cohen J, Cohen J, Gunsten S, Fréchet J, et al. Impact of hydrogel nanoparticle size and functionalization on in vivo behavior for lung imaging and therapeutics. Mol Pharm. 2009; 6:1891–902. [PubMed: 19852512]
35. Lee J, White A, Rice D, Smith B. In vivo imaging using polymeric nanoparticles stained with near-infrared chemiluminescent and fluorescent squaraine catenane endoperoxide. Chem Commun (Camb). 2013; 49:3016–8. [PubMed: 23467338]
36. Li K, Qin W, Ding D, Tomczak N, Geng J, Liu R, et al. Photostable fluorescent organic dots with aggregation-induced emission (AIE dots) for noninvasive long-term cell tracing. Sci Rep. 2013; 3
37. Liu Z, Rong P, Yu L, Zhang X, Yang C, Guo F, et al. Dual-Modality Noninvasive Mapping of Sentinel Lymph Node by Photoacoustic and Near-Infrared Fluorescent Imaging Using Dye Loaded Mesoporous Silica Nanoparticles. Mol Pharm. 2015; 12:3119–28. [PubMed: 26132789]
38. Ji X, Peng F, Zhong Y, Su Y, Jiang X, Song C, et al. Highly fluorescent, photostable, and ultrasmall silicon drug nanocarriers for long-term tumor cell tracking and in-vivo cancer therapy. Adv Mater. 2015; 27:1029–34. [PubMed: 25377423]
39. Miller M, Gadde S, Pfirschke C, Engblom C, Sprachman M, Kohler R, et al. Predicting therapeutic nanomedicine efficacy using a companion magnetic resonance imaging nanoparticle. Sci Transl Med. 2015; 7:314ra183.
40. Ding D, Mao D, Li K, Wang X, Qin W, Liu R, et al. Precise and Long-Term Tracking of Adipose-Derived Stem Cells and Their Regenerative Capacity via Superb Bright and Stable Organic Nanodots. ACS Nano. 2014; 8:12620–31. [PubMed: 25427294]
41. Chen P, Kang Y, Lin C, Chen S, Hsieh C, Chen Y, et al. Multitheragnostic Multi-GNRs Crystal-Seeded Magnetic Nanoseaurchin for Enhanced In Vivo Mesenchymal-Stem-Cell Homing, Multimodal Imaging, and Stroke Therapy. Adv Mater. 2015; doi: 10.1002/adma.201502784
42. Huang Z, Li C, Yang S, Xu J, Shen Y, Xie X, et al. Magnetic resonance hypointensive signal primarily originates from extracellular iron particles in the long-term tracking of mesenchymal

stem cells transplanted in the infarcted myocardium. Int J Nanomedicine. 2015; 10:1679–90. [PubMed: 25767388]

43. Manunta M, McAnulty R, McDowell A, Jin J, Ridout D, Fleming J, et al. Airway deposition of nebulized gene delivery nanocomplexes monitored by radioimaging agents. Am J Respir Cell Mol Biol. 2013; 49:471–80. [PubMed: 23614789]
44. Zhang K, Fang H, Wang Z, Taylor J, Wooley K. Cationic shell-crosslinked knedel-like nanoparticles for highly efficient gene and oligonucleotide transfection of mammalian cells. Biomaterials. 2009; 30:968–77. [PubMed: 19038441]
45. Fang H, Z K, Shen G, Wooley KL, Taylor JS. Cationic shell-cross-linked knedel-like (cSCK) nanoparticles for highly efficient PNA delivery. Mol Pharm. 2009; 6:615–26. [PubMed: 19231840]
46. Zhang K, Fang H, Wang Z, Li Z, Taylor J, Wooley K. Structure-Activity Relationships of Cationic Shell-crosslinked Knedel-like Nanoparticles: Shell Composition and Transfection Efficiency/ Cytotoxicity. Biomaterials. 2010; 31:1805. [PubMed: 19878990]
47. Samarajeewa S, Ibricevic A, Gunsten S, Shrestha R, Elsabahy M, Brody S, et al. Degradable Cationic Shell Cross-Linked Knedel-like Nanoparticles: Synthesis, Degradation, Nucleic Acid Binding, and In Vitro Evaluation. Biomacromolecules. 2013; 14:1018–27. [PubMed: 23510389]
48. Zhang K, Fang H, Wang Z, Li Z, Taylor JS, Wooley KL. Structure-activity relationships of cationic shell-crosslinked knedel-like nanoparticles: shell composition and transfection efficiency/ cytotoxicity. Biomaterials. 2010; 31:1805–13. [PubMed: 19878990]
49. Edwards W, Anderson C, Fields G, Welch M. Evaluation of radiolabeled type IV collagen fragments as potential tumor imaging agents. Bioconjug Chem. 2001; 12:1057–65. [PubMed: 11716700]
50. Sun X, Rossin R, Turner J, Becker M, Joralemon M, Welch M, et al. An assessment of the effects of shell cross-linked nanoparticle size, core composition, and surface PEGylation on in vivo biodistribution. Biomacromolecules. 2005; 6:2541–54. [PubMed: 16153091]
51. Yaghoubi S, Berger F, Gambhir S. Studying the biodistribution of positron emission tomography reporter probes in mice. Nat Protoc. 2007; 2:1752–5. [PubMed: 17641641]
52. Berezin, M. Nanotechnology for Biomedical Imaging and Diagnostics: From Nanoparticle Design to Clinical Applications. John Wiley & Sons; 2015.
53. Samarajeewa S, Zentay R, Jhurry N, Li A, Seetho K, Zou J, et al. Programmed hydrolysis of nanoassemblies by electrostatic interaction-mediated enzymatic-degradation. Chem Commun (Camb). 2014; 50:968–70. [PubMed: 24301076]
54. Shen Y, Fang H, Zhang K, Shrestha R, Wooley K, Taylor J. Efficient protection and transfection of small interfering RNA by cationic shell-crosslinked knedel-like nanoparticles. Nucleic Acid Ther. 2013; 23:95–108. [PubMed: 23557117]
55. Pouton C, Lucas P, Thomas B, Uduehi A, Milroy D, Moss S. Polycation-DNA complexes for gene delivery: a comparison of the biopharmaceutical properties of cationic polypeptides and cationic lipids. J Control Release. 1998; 53:289–99. [PubMed: 9741937]
56. Emi N, Kidoaki S, Yoshikawa K, Saito H. Gene Transfer Mediated by Polyarginine Requires a Formation of Big Carrier-Complex of DNA Aggregate. Biochem Biophys Res Commun. 1997; 231:421–4. [PubMed: 9070292]
57. Hunter A. Molecular hurdles in polyfectin design and mechanistic background to polycation induced cytotoxicity. Adv Drug Deliv Rev. 2006; 58:1523–31. [PubMed: 17079050]
58. Moghimi S, Symonds P, Murray J, Hunter A, Debska G, Szewczyk A. A two-stage poly(ethylenimine)-mediated cytotoxicity: implications for gene transfer/therapy. Mol Ther. 2005; 11:990–5. [PubMed: 15922971]
59. Gaspar V, de Melo-Diogo D, Costa E, Moreira A, Queiroz J, Pichon C, et al. Minicircle DNA vectors for gene therapy: advances and applications. Expert Opin Biol Ther. 2015; 15:353–79. [PubMed: 25539147]
60. Stenler S, Blomberg P, Smith C. Safety and efficacy of DNA vaccines: plasmids vs. minicircles. Hum Vaccin Immunother. 2014; 10:1306–8. [PubMed: 24553064]
61. Choi H, Ashitate Y, Lee J, Kim S, Matsui A, Insin N, et al. Rapid translocation of nanoparticles from the lung airspaces to the body. Nat Biotechnol. 2010; 28:1300–4. [PubMed: 21057497]

62. Sakagami M. In vivo, in vitro and ex vivo models to assess pulmonary absorption and disposition of inhaled therapeutics for systemic delivery. Adv Drug Deliv Rev. 2006; 58:1030–60. [PubMed: 17010473]

63. Dothager R, Goiffon R, Jackson E, Harpstrite S, Piwnica-Worms D. Cerenkov radiation energy transfer (CRET) imaging: a novel method for optical imaging of PET isotopes in biological systems. PLoS One. 2010; 510:e13300. [PubMed: 20949021]

64. Wang Y, Liu Y, Luehmann H, Xia X, Wan D, Cutler C, et al. Radioluminescent gold nanocages with controlled radioactivity for real-time in vivo imaging. Nano Lett. 2013; 13:581–5. [PubMed: 23360442]

65. Kotagiri N, Niedzwiedzki D, Ohara K, Achilefu S. Activatable probes based on distance-dependent luminescence associated with Cerenkov radiation. Angew Chem Int Ed Engl. 2013; 52:7756–60. [PubMed: 23765506]

66. McElvany K, Welch M. Characterization of Bromine-77-Labeled Proteins Prepared Using Bromoperoxidase. J Nucl Med. 1980; 21:953–60. [PubMed: 7420196]

67. Imbesi P, Raymond J, Tucker B, Wooley K. Thiolene “Click” Networks from Amphiphilic Fluoropolymers: Full synthesis and characterization of a benchmark anti-biofouling surface. J Mater Chem. 2012; 22:19462–73.

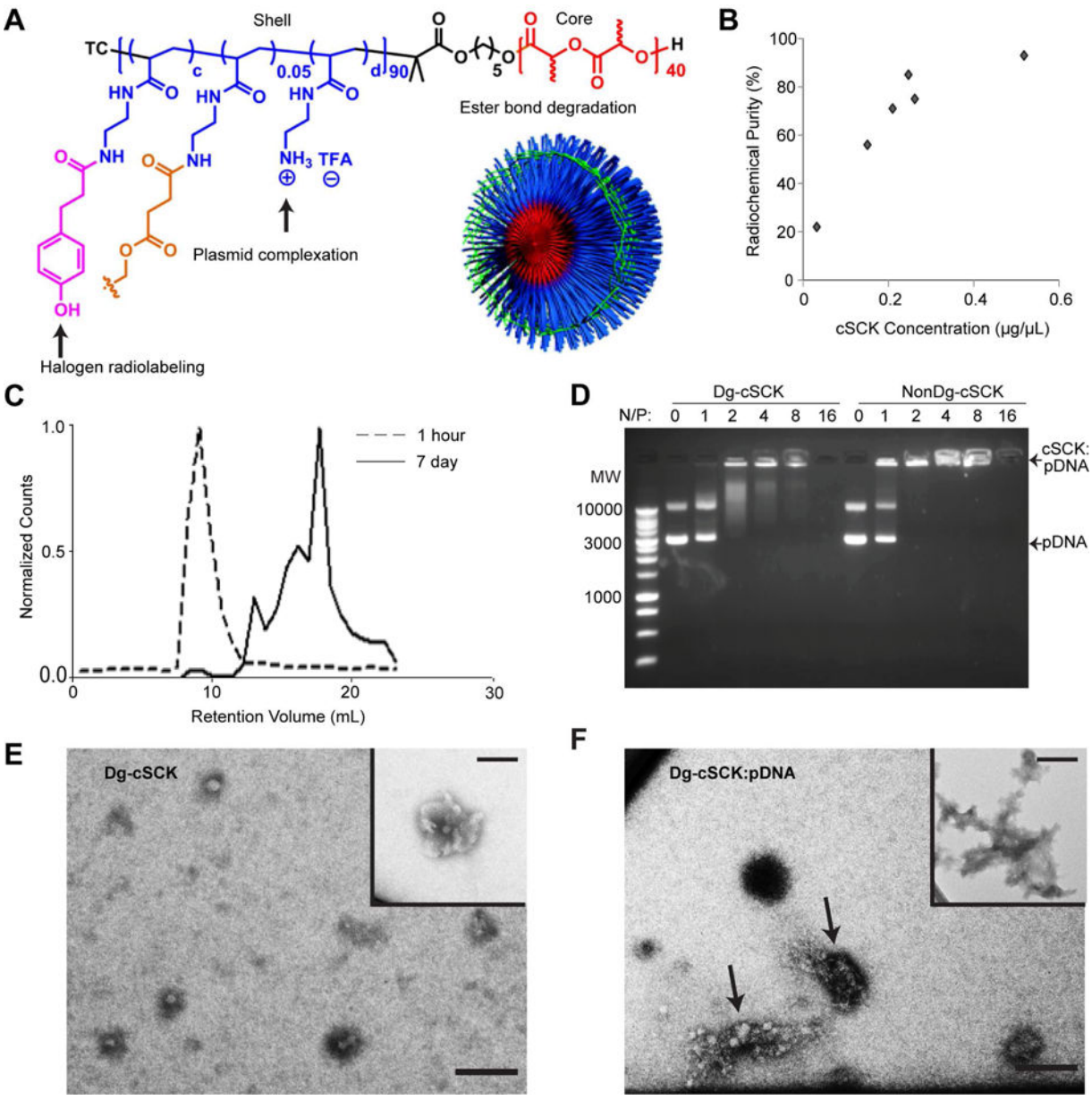

Figure 1. Multifunctional physicochemical features of degradable cSCKs

(A) Schematic of the chemical composition of the degradable cationic shell-cross-linked knedel-like nanoparticles (Dg-cSCKs), functionalized with a hydroxylated phenyl ring for halogen radiolabeling, amines for plasmid complexation, and ester bonds for degradation. A cartoon of the assembled Dg-cSCK shows crosslinkers in green. (B) Radiolabeling binding curve of ^{123}I onto Dg-cSCKs. (C) Degradation of Dg-cSCKs after 1 hour and 7 days in PBS, determined by fast protein liquid chromatography (FPLC). (D) Comparison of degradable cSCK and non-degradable cSCK binding to plasmid DNA (pDNA) detected by gel electrophoresis. Nanoparticles were combined at the indicated ratio of N/P amine (N) to pDNA phosphate (P) prior to gel electrophoresis. A molecular weight ladder is in the far left lane. TEM of (E) Dg-cSCK alone with an inset demonstrating aggregates of particles also observed and (F) nanocomplexes formed between Dg-cSCK and pDNA, with arrows

indicating two distinct complexes and an inset demonstrating an example of structures with different morphology that were also observed. Scale bar = 100 nm.

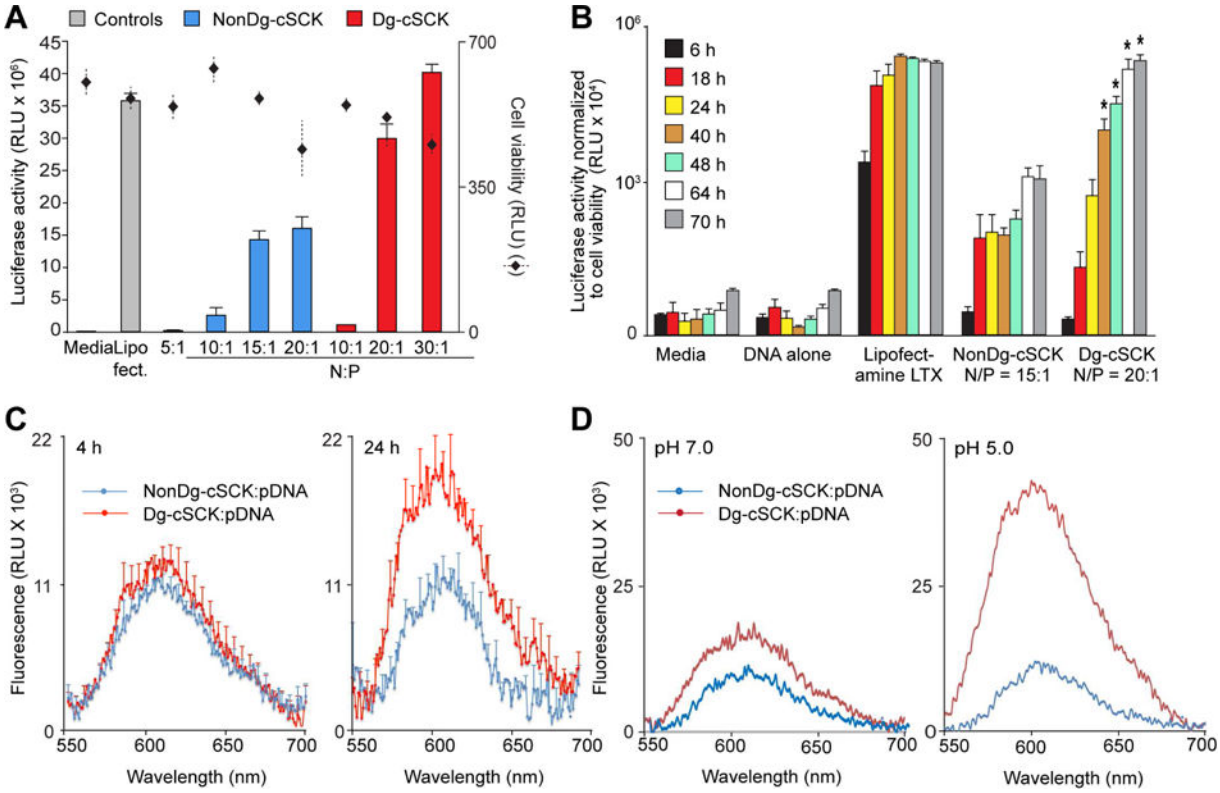

Figure 2. ***In vitro*** **characterization of pDNA transfection by cSCKs**

(A) Transfection efficiency and cell viability following transfection of HEK293T cells with a luciferase expression plasmid (pLuc*)* using the indicated conditions. Cell viability was determined using ATP activity. Shown are the luciferase and ATP activity as mean ± S.D. of triplicate samples from at least three independent experiments. (B) Time-dependent transfection efficiency of the indicated cSCK as determined by luciferase expression relative to cell viability. (C) Cell-free pDNA release from Dg-cSCK and NonDg-cSCK 4 (left) and 24 (right) hours after incubation in pH 7 buffer, detected using a Gel Red fluorescence assay to detect free DNA. (D) pH-dependent release of pDNA from Dg-cSCKs or NonDg-cSCKs, at indicated pH, detected at 24 h. C and D are representative of 3 experiments.

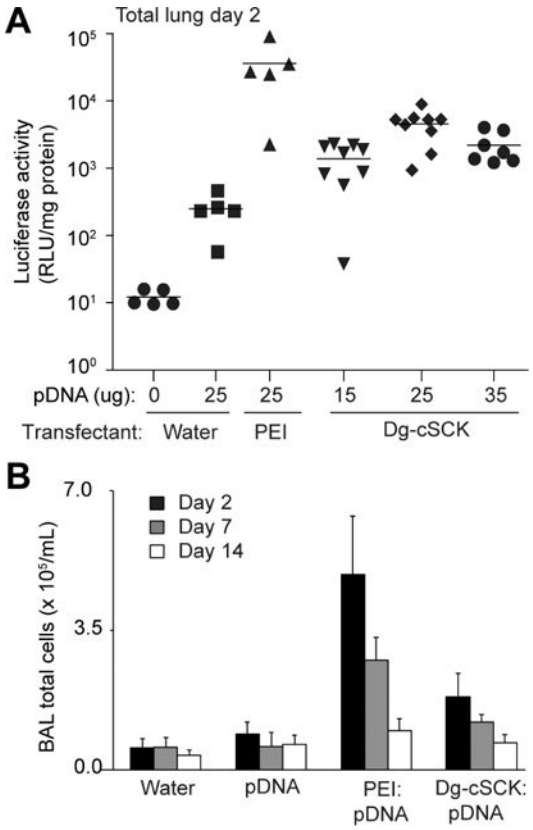

Figure 3. ***In vivo*** **transfection efficacy of Dg-cSCK in mouse lung**

Mice were dosed intratracheally with a Dg-cSCK complexed with a luciferase expression pDNA (pLuc) at the indicated conditions. Lungs were then subjected to bronchoalveolar lavage (BAL) and tissue was analyzed for luciferase activity and inflammatory cells. (A) Luciferase activity in whole lung adjusted for total protein concentration 2 days after intratracheal delivery of Dg-cSCK:pLuc nanocomplexes (N/P ratio 8:1). Each symbol represents a single animal. (B) Quantification of immune cells in BAL fluid after delivery of pDNA and nanocarriers at indicated days. Data are the mean ± S.D. of 3 to 9 mice for each condition.

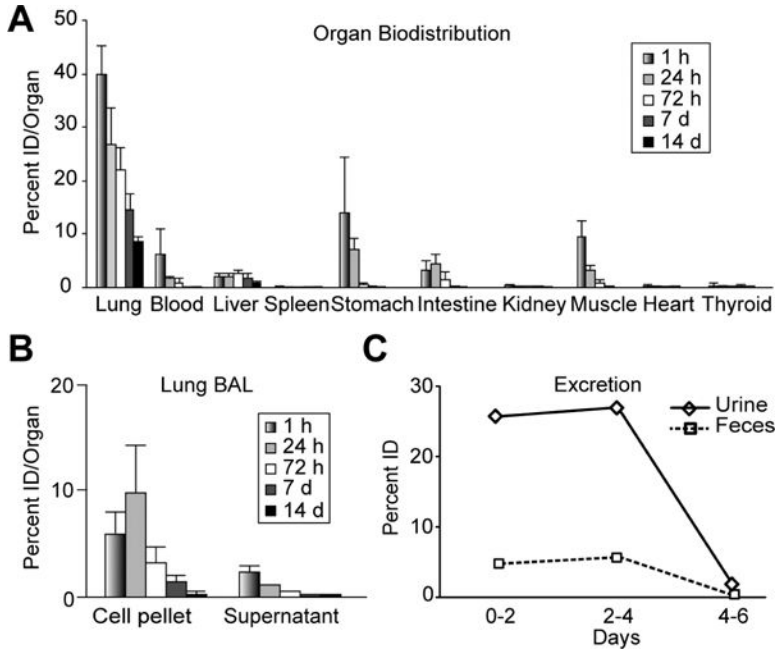

Figure 4. Quantitative biodistribution of ^{124}I-labeled Dg-cSCK complexed with luciferase expression pDNA (pLuc)

Intratracheal radiolabeled Dg-cSCK complexed with a luciferase expression pDNA (pLuc) were administered to mice and evaluated at the indicated time. (A) Organ distribution in percent ID/organ, (B) lung BAL distribution, and (C) quantitative excretion in feces and urine per day. A and B are the mean ± S.D. (n = 5 mice per time point) samples from 2 independent experiments. C is the average mean of activity per mouse based on a single sample from 5 mice co-housed in a metabolic cage.

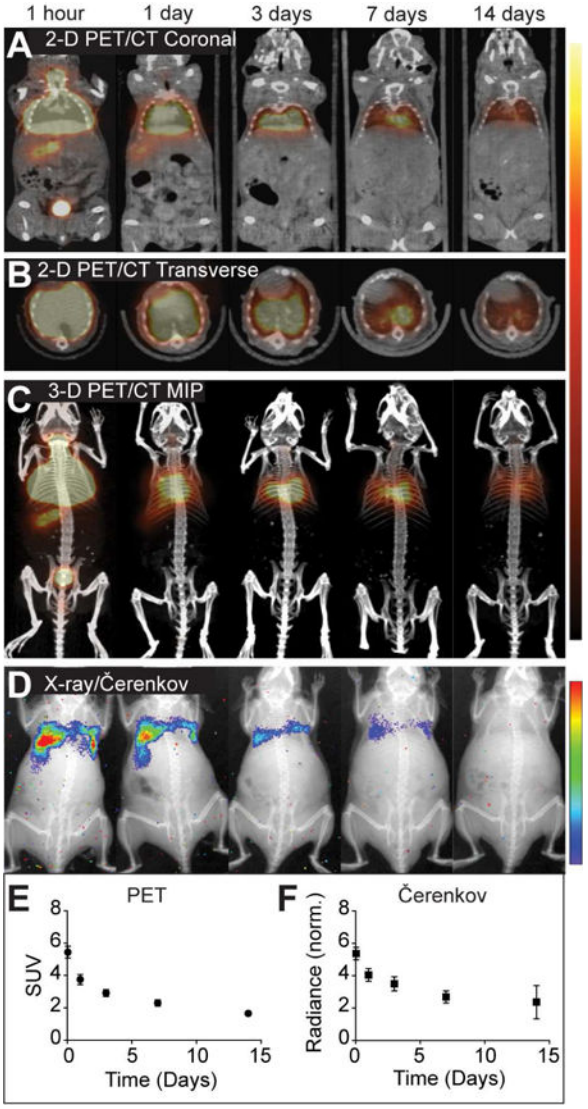

Figure 5. Multimodal imaging of ^{124}I-labeled cSCK-pDNA complexes

Representative images are shown at indicated times after intratracheal injection, of (A) 2-dimensional (2-D) PET/CT coronal slices, (B) 2-D PET/CT transverse slices, (C) PET/CT maximum intensity projections (MIPs), and (D) X-ray/Čerenkov luminescent imaging. The signal intensity scales are right of panel A–C and D. Image quantification of (E) standardized uptake values (SUV) from lung volumes in PET images and (F) normalized radiance from lung regions of interest, each corrected for ^{124}I decay over time. Shown are the mean ± S.D (n = 8).

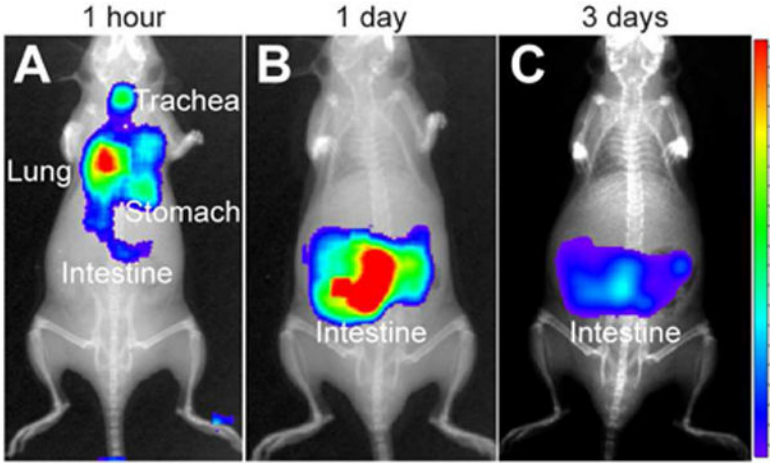

Figure 6.

Ĉerenkov imaging of Dg-cSCK:pDNA nanocomplex clearance. Mice were positioned in the supine position for luminescent imaging of ventral surface after intratracheal administration of 131I-labeled Dg-cSCK:pDNA nanocomplexes (A) immediately post administration, (B) after 3 days and (C) 7 days. The intensity scale is represented on the right.

Table 1

Performance of radiohalogens coupled to Dg-cSCK

Radio-halogen	Half-life	Specific activity	Dg-cSCK degradation studies	Bio-distribution studies	Imaging
^{123}I*	13 hours	932 MBq/mg	No	No	None
^{76}Br	16.2 hours	115 MBq/mg	No	Yes	PET/CT
^{124}I	4.2 days	137 MBq/mg	Yes	Yes	PET/CT, Čerenkov
^{131}I	8.0 days	292 MBq/mg	No	Yes	Čerenkov

* Used for optimization of radiohalogen labeling